Photoinduced electron transfer and geminate recombination on a micelle surface: Analytical theory and Monte Carlo simulations

Kristin Weidemaier and M. D. Fayer
Department of Chemistry, Stanford University, Stanford, California 94025

(Received 4 August 1994; accepted 23 November 1994)

A detailed theoretical analysis of photoinduced electron transfer and geminate recombination on the surface of a spherical micelle is presented. An exact point-particle analytical theory is first developed for one donor and N competing acceptors in random fixed positions on the micelle surface. The method is applicable to any restricted geometry system. Starting with a neutral donor and acceptors, the time dependent probability of having an excited neutral donor and the time dependent probability of having ions are calculated for various numbers of acceptors and various forward and back electron-transfer parameters. The theoretical results are compared to Monte Carlo simulations of the problem, and the exact agreement obtained demonstrates that the ensemble averages are properly performed. Comparison is also made to a previously reported approximate analytical theory. The analytical theory and the Monte Carlo simulations are then extended to include the effects of donor–acceptor and acceptor–acceptor excluded volume. Although donor–acceptor excluded volume may be included exactly, inclusion of acceptor–acceptor excluded volume renders the problem intractable. An approximate method of handling acceptor–acceptor excluded volume by utilizing the pair correlation function for the system is presented and compared to Monte Carlo simulations of the full problem. An approximate technique is suggested for generating the pair correlation function for curved disks on the surface of a sphere. © *1995 American Institute of Physics.*

I. INTRODUCTION

Electron-transfer reactions play critical roles in a wide variety of physical and biological processes and serve as key mechanisms for the harnessing of energy. As such, electron transfer has motivated numerous theoretical treatments aimed at predicting the time dependence of the process.[1–12] Yet in spite of the remarkable success of the Marcus theory[1–5] and its subsequent quantum mechanical extensions,[13–17] it has remained difficult to predict the full time scale of electron transfer processes when transfer can occur to any of a number of acceptors, all competing for the electron, and when geminate recombination is included in the dynamical problem. For photoinduced electron transfer in isotropic three dimensions, several different theoretical approaches have been developed, most of which make substantial approximations that simplify the many-body nature of the process.[8,9,12,18,19] An exact treatment of the problem is, however, possible. When the distance dependence of the electron transfer rate is modeled as falling off exponentially,[20–23] the many-body problem of forward electron transfer for fixed particles distributed in infinite three dimensions has been treated rigorously.[7] An exact method for including back electron transfer (geminate recombination) has also been obtained[10,11,24] and has been compared with the approximate treatments in a recent article.[25] The exact results are amenable to fairly simple numerical analysis.

There have been a number of recent attempts to treat electron transfer reactions in restricted geometries.[26–28] This is an important and interesting problem since electron transfer in systems like micelles, zeolites, and polymers can be strongly affected by the restricted, nonisotropic nature of the spatial structure, and controlling the geometry may ultimately provide a means of regulating the rate of electron transfer and geminate recombination. To date, however, theoretical models of the restricted geometry problem have made use of many of the same simplifying approximations utilized in isotropic three dimensions.[28] Such approximations may be no more valid in restricted geometry systems than they are in infinite volume ones. Since an exact method does exist for infinite three dimensional systems, it is reasonable to extend this method to the problem of restricted geometries.

In this article, we develop an exact theoretical method for treating the dynamics of photoinduced forward electron transfer with geminate recombination in restricted geometries. We specifically consider the problem of one donor and N acceptors distributed on the surface of a spherical micelle, but the method is applicable to any spatial structure. The model calculations of the dynamics of photoinduced electron transfer and geminate recombination on the surface of a micelle are the first accurate calculations of the electron-transfer problem in a restricted geometry. They permit comparison to analogous exact calculations for infinite three dimensional systems so that the role of donor and acceptor clustering in a restricted geometry may be understood. The analytical results allow the effects of the micelle curvature and the finite number of acceptors to be studied and are sufficiently general to permit comparison of electron transfer events in a wide variety of restricted geometries.

To verify the accuracy of our theory, we have performed detailed Monte Carlo simulations of electron transfer between one donor and N acceptors on the surface of a micelle. The simulations and the theory show perfect agreement. Furthermore, because a physical system will consist of an ensemble of micelles, each with its own arrangement of acceptors about the donor, the analytical theory must correctly

 0021-9606/95/102(9)/3820/10/$6.00

perform the averages over all possible acceptor configurations. The agreement between theory and simulation then demonstrates unambiguously that the ensemble averages have been properly performed.

The initial calculations presented here, like those in other electron-transfer calculations,[7–9,12,19] assume that the donor and acceptors are point particles. Real molecules, however, have finite sizes, and therefore it is important to assess the role of excluded volume on the dynamics of electron transfer in the micelle problem. Excluded volume limits the distance of closest approach of an acceptor to the donor (donor–acceptor excluded volume) and it eliminates from the spatial distribution those configurations in which acceptors physically overlap (acceptor–acceptor excluded volume). Donor–acceptor excluded volume is important at all concentrations of acceptors and is handled exactly by the analytical theory presented here (as in Refs. 7–9,12,19) by performing the ensemble average over acceptor configurations with a short distance cutoff. When donor–acceptor excluded volume is included, theory and simulation again yield exact agreement. Acceptor–acceptor excluded volume, however, cannot be treated exactly, and an approximate method is instead developed that takes acceptor–acceptor excluded volume into account through a pair correlation function. The accuracy of this approximation can be studied by comparing the approximate analytical results with Monte Carlo simulations in which all types of excluded volumes have been rigorously included.

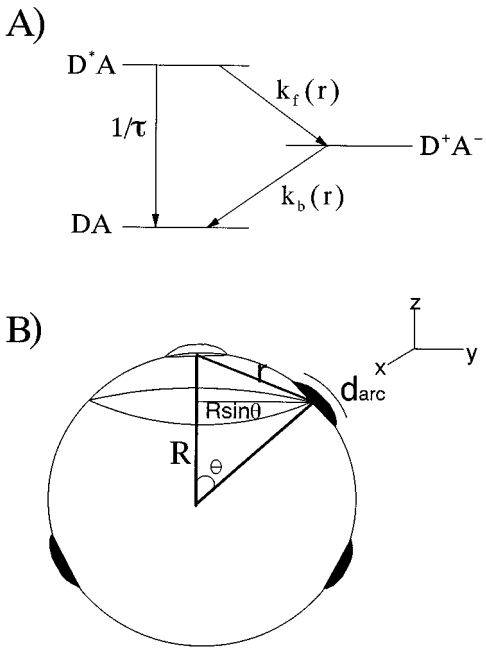

FIG. 1. (A) A diagram of the three level electron-transfer system. Shown are the ground (DA), excited (D^*A), and ionic (D^+A^-) states. The three rate processes are represented by their rates, $1/\tau$, $k_f(r)$, and $k_b(r)$, which are the inverse fluorescence lifetime of the donor and the forward and back transfer rates, respectively. (B) A pictorial representation of the micelle system. The micelle is modeled as a hard sphere of radius R. The donor and acceptors are hard curved disks with arclengths, $d_{\rm arc}$. Acceptors are shown as solid-filled disks, while the donor is the unfilled disk. The relevant electron-transfer distance is the chord length r.

II. THE MODEL AND MONTE CARLO TECHNIQUES

The electron-transfer system modeled here is a three level system in which photoexcitation of the donor may be followed either by direct relaxation to the ground state (excited state lifetime) or by electron transfer to one of the spatially distributed acceptors. After forward electron transfer occurs, the donor and the acceptor with the electron will exist as ions, with charges determined by their initial pretransfer charges. We term this the charge-transfer state, and for conciseness, consider initially neutral donor and acceptors so that electron transfer results in the creation of a donor cation and acceptor anion. The model and results, though, are completely general, provided that the initial donor and acceptor distribution is not influenced by the pretransfer charges on the particles. A straightforward extension can include any type of initial spatial distribution. In a solid solution (no diffusion), the acceptor with the electron will eventually back transfer to the original donor, thereby regenerating the ground state. [See Fig. 1(A).] Acceptor concentration is assumed to be much higher than donor concentration, so we consider the case where there is only one donor per micelle. Therefore, back transfer occurs only to the original donor. Electron transfer from the acceptor anion to a nearby neutral acceptor is not considered since there is no net driving force for the process, and barriers for electron tunneling are generally large.[29] The micelles are taken to be dilute, so that electron transfer from a donor on one micelle to an acceptor on another micelle is not considered. However, micelle-to-micelle excitation transfer has been studied in detail,[30,31] and this electron-transfer theory could be extended in an analogous manner.

The micelle is modeled as a hard sphere of radius R, while the donor and acceptors exist as hard curved disks of arclength $d_{\rm arc}$ embedded on the surface of the sphere.[32] (Initially, $d_{\rm arc}=0$ for point particles.) The relevant electron-transfer distance is the through-sphere (chord) distance, r. [See Fig. 1(B).] Diffusion is not here considered.

The Monte Carlo simulations were performed by first placing the donor and N acceptors randomly on the surface of the sphere. Spherical coordinates were used, and particle positions were chosen randomly to satisfy[31]

$$\theta=\arccos[1-2f], \quad \phi=2\pi f,$$

where θ is the polar angle, ϕ the azimuthal angle, and f is a random number generated uniformly on (0,1). The theta distribution must have an arccos dependence on f since a particle is more likely to exist at the equator than at the poles. The random numbers were generated using the algorithm by Marsaglia and Zaman, which has a period of about 10^8.[33] The algorithm utilizes 24 input seed numbers obtained from a second, shorter period generator, and 10 000 unused calls were made to the generator to eliminate any initial bias from the seeds.[34]

The finite size of the particles was included in the simulations in two distinct yet equivalent ways. For low packing fractions, the particles were placed sequentially, and particle overlap was checked after each placement. When a newly

placed particle overlapped any of the other particles, the entire configuration was regenerated, beginning again with the placement of the first particle. For higher packing fractions, the particles were again placed sequentially. This time, however, when the ith particle overlapped any of the others, it was merely replaced until it no longer overlapped. Placement then resumed with the ith+1 particle. Configurations generated this second way do not reproduce the equilibrated distribution[35–38] since the particles placed last are heavily affected by the positions of the earlier-placed particles, while the earlier particles feel no effect from the later particles. When particles are placed in this second way, the entire system must be equilibrated.[35–38] The equilibrated configuration is then used.

The first method of rejecting entire configurations when placing the particles, but omitting equilibration, is exactly equivalent to placing the particles in the second way and then equilibrating the system.[39] Extensive testing of both methods was performed, and both were found to give the same results. At low concentrations, the first method was used. At higher concentrations, though, the second method was used for computational efficiency.

Equilibration was performed by transforming to a coordinate system in which the particle to be moved was at the north pole. The particle then stepped a fixed length in a random ϕ direction, and the new position was transferred back to the original coordinate system. When stepping led to overlap with another particle, the move was rejected. Step sizes were chosen to give an average rejection fraction of 50%. The total number of steps taken per configuration was between 10^3 and 10^4. In all cases, increasing the number of steps by a factor of 10 led to the same results, demonstrating that a sufficient number of steps was utilized.

Micelle systems with fractional occupancies ranging from 0% to 20% were considered. These occupancies were obtained by varying both the size of the micelle and the size and number of acceptors. Typical micelle radii range from 18 Å (sodium dodecyl sulfate) to 42 Å (Triton X-100), while typical acceptors have radii ranging from 3 to 10 Å. These physical considerations may make fractional occupancies greater than 10% difficult to achieve experimentally.

Simulations were performed on an IBM RS6000 model 375 workstation. Simulation times ranged from 5–15 hours depending on acceptor concentration. In all cases, great care was taken to ensure convergence. This usually required the generation of between 10^5 and 10^6 configurations.

III. THE ANALYTICAL THEORY

A. Forward transfer

We take a standard approach[20–23] and model the electron-transfer rate constants as exponentially decaying functions of distance

$$k = 1/\tau, \tag{1}$$

$$k_f(r) = (1/\tau)\exp[(R_f - r)/a_f], \tag{2}$$

$$k_b(r) = (1/\tau)\exp[(R_b - r)/a_b], \tag{3}$$

where $k_f(r)$ and $k_b(r)$ are the rate constants for the forward and back transfer, respectively, k is the rate constant for excited donor relaxation to the ground state in the absence of electron transfer, and τ is the donor excited-state lifetime. [See Fig. 1(A).] R_f, a_f, R_b, and a_b are parameters that characterize the distance scales of the forward and back electron transfer, and $1/\tau$ is used as an arbitrary scaling constant for $k_f(r)$ and $k_b(r)$.[10,11,40]

We begin by considering a specific random configuration of 1 donor and N acceptors on the surface of a micelle. The configuration is denoted by $\bar{r} = r_1, r_2, r_3, \ldots, r_N$, indicating that acceptor 1 is at distance r_1 from the donor, acceptor 2 at distance r_2, etc. The position of the donor is arbitrary, and the coordinate system is chosen so that the donor is at the north pole.

If the donor is optically excited at time $t = 0$, then the probability that the donor will still be excited at some time t later, $P_{\mathrm{ex}}(\bar{r},t)$, follows the master equation

$$\frac{\partial P_{\mathrm{ex}}(\bar{r},t)}{\partial t} = -\left(\frac{1}{\tau} + \sum_{i=1}^{N} k_f(r_i)\right) P_{\mathrm{ex}}(\bar{r},t), \tag{4}$$

which gives

$$P_{\mathrm{ex}}(\bar{r},t) = \exp\left(\frac{-t}{\tau}\right)\exp\left(-\sum_{i=1}^{N} k_f(r_i)t\right). \tag{5}$$

This is the excited-state survival probability for the specific configuration $\bar{r}$.

A physical system will consist of an ensemble of such configurations, and the observable will be the ensemble average of $P_{\mathrm{ex}}(\bar{r},t)$, defined as

$$\langle P_{\mathrm{ex}}(t)\rangle = \int_{r_1}\int_{r_2}\cdots\int_{r_N} P_{\mathrm{ex}}(\bar{r},t)p(\bar{r})dr_1\, dr_2\cdots dr_N, \tag{6}$$

where $p(\bar{r})$ is the probability of configuration $\bar{r}$ occurring. For point particles, the positions of the N acceptors are uncorrelated, and thus the probability distribution $p(\bar{r})$ is separable such that $p(\bar{r}) = p(r_1)p(r_2)\cdots p(r_N) = p(r)^N$ and

$$\langle P_{\mathrm{ex}}(t)\rangle = \exp\left(\frac{-t}{\tau}\right)\left[\int_{r=0}^{2R} e^{-k_f(r)t}p(r)dr\right]^N, \tag{7}$$

where N is the number of acceptors and $p(r)$ is the probability that any given acceptor is at distance r from the donor. The upper limit of integration is the maximum chord length, or $2R$ for a micelle of radius R.

The complete spatial dependence lies in $p(\bar{r}) = p(r_1, r_2, \ldots, r_N)$, or for point particles, simply in $p(r)$. For point particles in isotropic three dimensions

$$p(r)dr = \frac{4\pi r^2}{V}\, dr$$

for a spherical volume V with the donor at the center.[41] For point particles on the surface of a micelle (see Appendix A),

$$p(r)dr = (r/2R^2)dr. \tag{8}$$

The integral equation for $\langle P_{\mathrm{ex}}(t)\rangle$ with $p(r)dr = r\, dr/2R^2$ has no analytical solution and must be solved numerically.

B. Back transfer (forward transfer with geminate recombination)

Calculation of the survival probability of the donor cation is substantially more complicated than the forward transfer calculation since the cation survival probability is determined by the details of the forward transfer. A complete theoretical treatment has already been developed for an infinite three dimensional system.[10,11,40] If $P^i_{ct}(\bar{r},t)$ is the probability that the donor is still a cation at time t with the ith acceptor an anion and the N acceptors located at r_1, $r_2,\ldots,r_N$, then

$$\frac{\partial P^i_{ct}(\bar{r},t)}{\partial t}=k_f(r_i)P_{ex}(\bar{r},t)-k_b(r_i)P^i_{ct}(\bar{r},t). \tag{9}$$

Directly solving this equation gives

$$P^i_{ct}(\bar{r},t)=\frac{k_f(r_i)}{(1/\tau)-k_b(r_i)+\sum_{j=1}^{N}k_f(r_j)}\left\{\exp[-k_b(r_i)t]-\exp\left(\frac{-t}{\tau}\right)\exp\left[-\sum_{j=1}^{N}k_f(r_j)t\right]\right\}. \tag{10}$$

The ensemble average of Eq. (10) cannot be performed directly, but it can be performed exactly using the procedure of Lin *et al.*[10,11,40] Equation (9) is first ensemble averaged over the $N-1$ acceptors without the electron and then solved for $\langle P^i_{ct}(r,t)\rangle_{N-1}$.

$$\langle P^i_{ct}(r,t)\rangle_{N-1}=\int_0^t k_f(r)e^{-k_b(r)(t-t')}\langle P_{ex}(r,t')\rangle_{N-1}\,dt', \tag{11}$$

where $\langle\ \rangle_{N-1}$ denotes the ensemble average over the $N-1$ acceptors which do not participate in the transfer. Since

$$\langle P_{ex}(r,t')\rangle_{N-1}=\exp\left(\frac{-t'}{\tau}\right)\exp[-k_f(r)t']\left[\frac{1}{2R^2}\times\int_{r'=0}^{2R}\exp\left[\frac{-t'}{\tau}\,e^{(R_f-r')/a_f}\right]r'\,dr'\right]^{N-1}$$

substituting into Eq. (11) and integrating over the remaining spatial coordinate gives

$$\langle P^i_{ct}(t)\rangle=\int_{r=0}^{2R}\int_{t'=0}^{t}k_f(r)\exp\left(\frac{-t'}{\tau}\right)\exp[-k_f(r)t']\times\exp[-k_b(r)(t-t')]\left[\int_{r'=0}^{2R}\exp\left[\frac{-t'}{\tau}\times e^{(R_f-r')/a_f}\right]\frac{r'}{2R^2}\,dr'\right]^{N-1}dt'\,\frac{r}{2R^2}\,dr. \tag{12}$$

Note that, unlike the infinite three dimensional case, the thermodynamic limit is not taken for the restricted geometry problem because the number of particles is finite. Equation (12) is the probability of finding the donor as a cation with the ith acceptor the anion. The total probability of finding the donor in its ionic state with any one of the acceptors with the electron is obtained by summing $\langle P^i_{ct}(t)\rangle$ over the N acceptors

$$\langle P_{ct}(t)\rangle=\sum_{i=1}^{N}\langle P^i_{ct}(t)\rangle=N\langle P^i_{ct}(t)\rangle. \tag{13}$$

Equation (13) is an exact solution to the problem for point particles.

Equations (7) and (13) were derived assuming a separable N-particle probability distribution, $p(\bar{r})=p(r_1)p(r_2)\cdots p(r_N)$, or that the probability of finding the ith particle between $r_j-\Delta r_j/2$ and $r_j+\Delta r_j/2$ is independent of the locations of the other $N-1$ particles. This is true for point particles. Real particles, however, have finite sizes, and the particle positions are not independent since no more than one particle can occupy the same region of space. There are two types of particle interactions involved: donor–acceptor and acceptor–acceptor. The finite size of the donor and acceptors limits the distance of closest approach of an acceptor to the donor. Since donor–acceptor excluded volume excludes short distances and since these short distances have the greatest impact on the electron transfer event, donor–acceptor excluded volume has a much larger effect on the electron transfer survival probability than does acceptor–acceptor excluded volume.

Donor–acceptor excluded volume is included by incorporating a cutoff in the integral to limit the distance of closest approach to r_m, the donor–acceptor contact distance in chord length. The probability distribution must be properly renormalized. (See Appendix A.) Except for the cutoff, acceptors are still modeled as point particles, and $p(\bar{r})=p(r_1,r_2,\ldots,r_N)$, which gives the probability distribution for the acceptors, remains separable. For this model (donor–acceptor excluded volume but no acceptor–acceptor excluded volume) the analytical theory is still exact and gives

$$\langle P_{ex}(t)\rangle=\exp\left(\frac{-t}{\tau}\right)\left[\frac{2}{4R^2-r_m^2}\int_{r_m}^{2R}\exp[-k_f(r)t]r\,dr\right]^N, \tag{14}$$

$$\langle P_{ct}(t)\rangle=\frac{2N}{4R^2-r_m^2}\int_{r=r_m}^{2R}\int_{t'=0}^{t}k_f(r)\exp\left(\frac{-t'}{\tau}\right)\times\exp[-k_f(r)t']\exp[-k_b(r)(t-t')]\times\left[\frac{2}{4R^2-r_m^2}\int_{r'=r_m}^{2R}\exp\left[\frac{-t'}{\tau}\,e^{(R_f-r')/a_f}\right]r'\times dr'\right]^{N-1}dt'\,r\,dr. \tag{15}$$

No approximations have been used, and the full distance dependence of the reaction is properly handled. An approximate treatment of acceptor–acceptor excluded volume is given below.

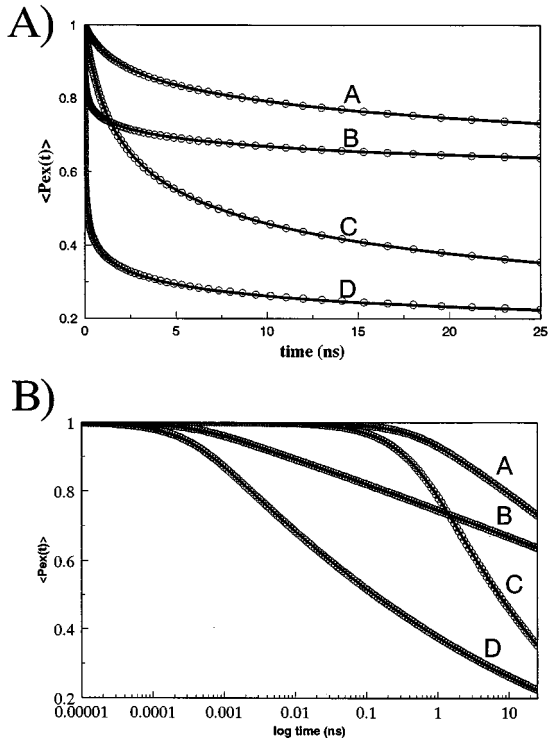

FIG. 2. $\langle P_{ex}(t)\rangle$ curves from Monte Carlo simulations and the analytical theory [Eq. (14)]. The Monte Carlo results are the open circles, while the solid lines are the theoretical results. The curves are plotted linearly in time (Part A) and logarithmically in time (Part B). Lifetime decay is not included. For both (A) and (B), the electron-transfer parameters are as follows: Curve A: $N=6$, $R_f=10.0$ Å, $a_f=1.0$ Å, $\tau=15.0$ ns; Curve B: $N=6$, $R_f=12.0$ Å, $a_f=0.5$ Å, $\tau=15.0$ ns; Curve C: $N=20$, $R_f=10.0$ Å, $a_f=1.0$ Å, $\tau=15.0$ ns; Curve D: $N=20$, $R_f=12.0$ Å, $a_f=0.5$ Å, $\tau=15.0$ ns. All curves are for a micelle of radius 20 Å, with point-particle acceptors, and a 6.8 Å donor–acceptor contact distance.

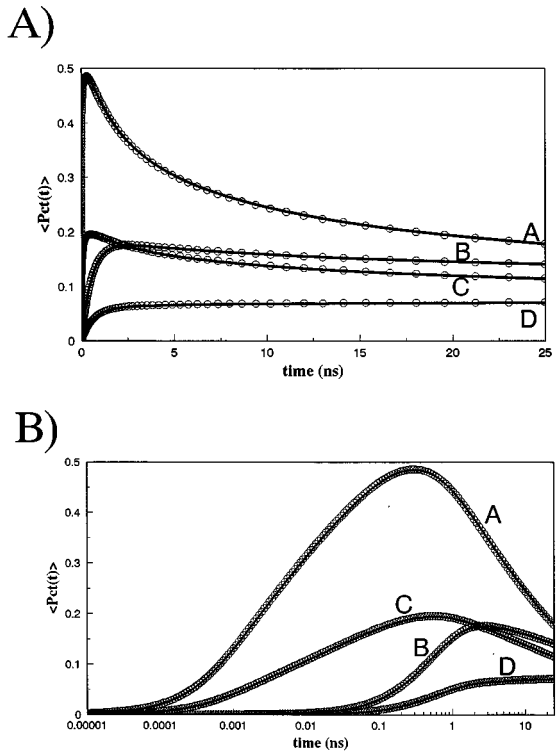

FIG. 3. $\langle P_{ct}(t)\rangle$ curves from Monte Carlo simulations (circles) and the analytical theory [Eq. (15), solid lines]. The curves are shown without lifetime decay and are plotted linearly (Part A) and logarithmically (Part B) in time. The parameters are: Curve A: $N=20$, $R_f=12.0$ Å, $a_f=0.5$ Å, $R_b=10.0$ Å, $a_b=1.0$ Å, $\tau=15.0$ ns; Curve B: $N=20$, $R_f=10.0$ Å$=R_b$, $a_f=1.0$ Å$=a_b$, $\tau=15.0$ ns; Curve C: $N=6$, $R_f=12.0$ Å, $a_f=0.5$ Å, $R_b=10.0$ Å, $a_b=1.0$ Å, $\tau=15.0$ ns; Curve D: $N=6$, $R_f=10.0$ Å$=R_b$, $a_f=1.0$ Å$=a_b$, $\tau=15.0$ ns. All curves are for a micelle of radius 20 Å, with point-particle acceptors and a 6.8 Å donor–acceptor contact distance.

IV. RESULTS AND DISCUSSION

The theoretical results given in Sec. III are exact and should yield perfect agreement with Monte Carlo simulations based on the same model of electron transfer. To verify this, Monte Carlo simulations with donor–acceptor excluded volume were performed. The Monte Carlo simulations generate a large number of configurations of point-particle acceptors but with a short distance cutoff of r_m. For each configuration, $P_{ex}(\bar{r},t)$ is calculated from Eq. (5), while $P_{ct}(\bar{r},t)$ is obtained by calculating $P_{ct}^{i}(\bar{r},t)$ for each acceptor [Eq. (10)] and summing over the N acceptors. The $P_{ex}(\bar{r},t)$ and $P_{ct}(\bar{r},t)$ curves for each configuration are then averaged. This should correspond exactly to the analytical $\langle P_{ex}(t)\rangle$ and $\langle P_{ct}(t)\rangle$ curves obtained from Eqs. (14) and (15).

Figure 2 shows simulated and analytical $\langle P_{ex}(t)\rangle$ curves for 6 and 20 acceptors on a 20 Å radius micelle for two sets of electron-transfer parameters. (See figure caption for parameters.) The curves are plotted on both linear and logarithmic time scales to better illustrate the full time dependence of the process. Both sets of curves are shown without donor lifetime decay, since donor lifetime is included simply by multiplying by $\exp(-t/\tau)$. The $\exp(-t/\tau)$ factor, however, can obscure the dynamics of the electron transfer, and thus curves are shown without it. As can be seen in the figure, the Monte Carlo and analytical curves are indistinguishable.

In the log plot at very short time, the curves are almost flat. Because of donor–acceptor excluded volume, there is a distance of closest approach and therefore a maximum forward transfer rate. On time scales short compared to the inverse of the maximum transfer rate, there are essentially no dynamics. The $\langle P_{ex}(t)\rangle$ curves (excited donor probability) have an interesting shape. The dynamics can be seen to span a very wide range of times when viewed in this manner. The shapes of these curves are distinctly different from the equivalent curves for infinite three dimensional systems.[41] This is indicative of the role that the restricted geometry plays in the dynamics of electron transfer.

Figure 3 shows simulated and analytical $\langle P_{ct}(t)\rangle$ curves for $N=6$ and $N=20$ for two sets of electron-transfer parameters. The donor lifetime decay has not been included in order to emphasize the electron-transfer dynamics. Again, both linear and logarithmic time scale plots are shown with forward and back electron-transfer parameters given in the figure caption. For fixed R_f, a_f, R_b, and a_b, the total number of ions formed increases with the number of acceptors because more acceptors are available for transfer. The $\langle P_{ct}(t)\rangle$ curves build in from zero as ions are generated by forward transfer. As time goes on, these ions begin to back

transfer even as new ions continue to be created from the forward transfer. At very short times, most of the ions formed will be at short distances, leading to swift back transfer, while at longer times, forward transfer to longer distances begins to occur, resulting in longer-lasting ions. The complex interplay between these processes determines the height and location of the maximum. A wide range of parameters has been studied, and in all cases the agreement between the simulation and the exact theory is perfect. This is the most important test of the theory. The forward transfer is relatively straightforward to deal with even in restricted geometries. However, to understand the dynamics of ion formation and recombination, it is necessary to include the geminate recombination correctly. The procedure of Lin *et al.*, which was developed for infinite three dimensional systems in the thermodynamic limit, can now be applied to restricted geometry problems.

There has been an approximate theoretical treatment of electron transfer with geminate recombination[12] that has recently been extended to restricted geometries.[28] This work modeled electron transfer assuming rate constants given by Eqs. (1)–(3) and accepting the form of master Eqs. (4) and (9). However, these authors use approximations that simplify the full many-body nature of the problem. For the infinite three dimensional problem, this approximate method was found to be accurate only in the limit of extremely low acceptor concentration, i.e., when the acceptor concentration approaches zero.[25] A similar inaccuracy also occurs in the restricted geometry problem. Both the approximate method of Ref. 28 and the exact theory presented here treat the forward transfer in the same manner. Any difference in the results is thus due to the approximations used in handling geminate recombination. $\langle P_{\mathrm{ct}}(t)\rangle$ curves calculated by the two methods are shown in Fig. 4 for 6 acceptors (upper panel) and 20 acceptors (lower panel) on a 20 Å radius micelle. (See figure caption for electron-transfer parameters.) Also shown are the Monte Carlo simulations (the circles in the figure). The solid lines through the Monte Carlo results are the $\langle P_{\mathrm{ct}}(t)\rangle$ curves calculated from the exact theory presented here, while the dashed lines were calculated using the approximate theory of Ref. 28. The donor lifetime decay is not included in any of the calculations. For all values of the electron-transfer parameters, the approximate curves show pronounced deviations from the Monte Carlo simulated results and from the exact theory curves, which are indistinguishable from the simulations. The approximation does improve as the number of acceptors is reduced, but remains poor even for only 5 or 6 acceptors on the micelle.

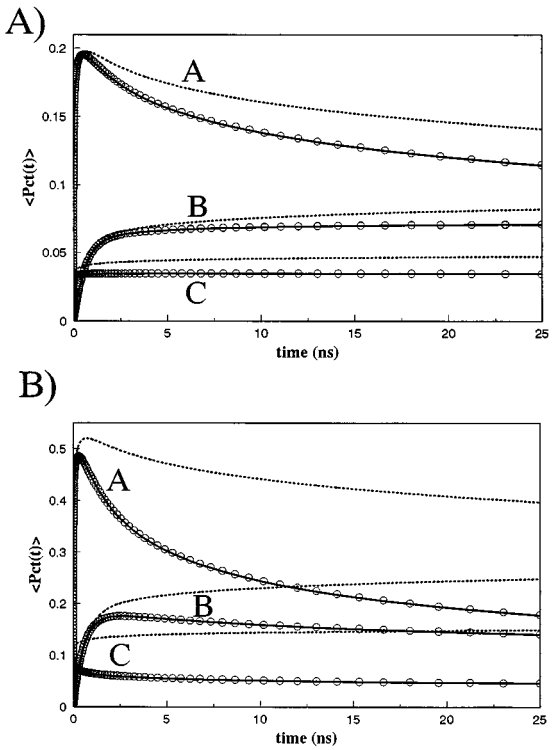

FIG. 4. Simulated $\langle P_{\mathrm{ct}}(t)\rangle$ curves (circles) compared with the analytical theory presented here [Eq. (15)—solid lines] and with the approximate theory used in Ref. 28 (dashed lines). Part A is for $N=6$, and Part B is for $N=20$. All curves are for $R=20$ Å, point-particle acceptors, and a 6.8 Å donor–acceptor contact distance. Parameter are: Curve A: $R_f=12.0$ Å, $a_f=0.5$ Å, $R_b=10.0$ Å, $a_b=1.0$ Å, $\tau=15.0$ ns; Curve B: $R_f=10.0$ Å$=R_b$, $a_f=1.0$ Å$=a_b$, $\tau=15.0$ ns; Curve C: $R_f=12.0$ Å$=R_b$, $a_f=0.5$ Å$=a_b$, $\tau=15.0$ ns. Donor lifetime decay is not included.

V. INCLUSION OF ACCEPTOR–ACCEPTOR EXCLUDED VOLUME

As long as the acceptors are assumed to be point particles, the analytical theory presented above [Eqs. (14) and (15)] is exact. Real acceptors, however, have finite size, and acceptor–acceptor excluded volume can be important. Configurations in which two or more acceptors overlap should not be included in the ensemble average. Furthermore, for any real physical system, the positions of the N acceptors are not independent but are highly correlated, as revealed by the oscillations in the pair distribution functions for finite-volume particles in infinite three dimensional systems.[35,36,38,42–44] Thus, for finite-sized acceptors, $p(\bar{r})=p(r_1,r_2,\ldots,r_N)$ can no longer be factored. The method of Lin *et al.* that reduces the many-body problem to a two-body problem cannot be used. More fundamentally, the necessary N-particle distribution function is not known, and therefore an exact analytical theory is not obtainable.

By comparing analytical theory without acceptor–acceptor excluded volume to Monte Carlo simulations including this effect, the role of acceptor–acceptor excluded volume can be studied. Figures 5(a) and 5(b) show a typical comparison for a 20 Å radius micelle with 10% of its surface area occupied by acceptors. $\langle P_{\mathrm{ex}}(t)\rangle$ and $\langle P_{\mathrm{ct}}(t)\rangle$ curves are shown in Figs. 5(a) and 5(b), respectively, with the Monte Carlo results depicted by circles and the analytical theory by the uppermost sets of solid lines. (The dashed lines are an approximate result to be discussed below.) The analytical theory shows some deviation from the Monte Carlo simulations due to its neglect of acceptor–acceptor excluded volume. The extent of this deviation will depend on the fraction of the micelle surface occupied by acceptors (fractional occupancy, η) as well as on the electron-transfer parameters themselves. While we have not performed an exhaustive study of all combinations of parameters, we do in general

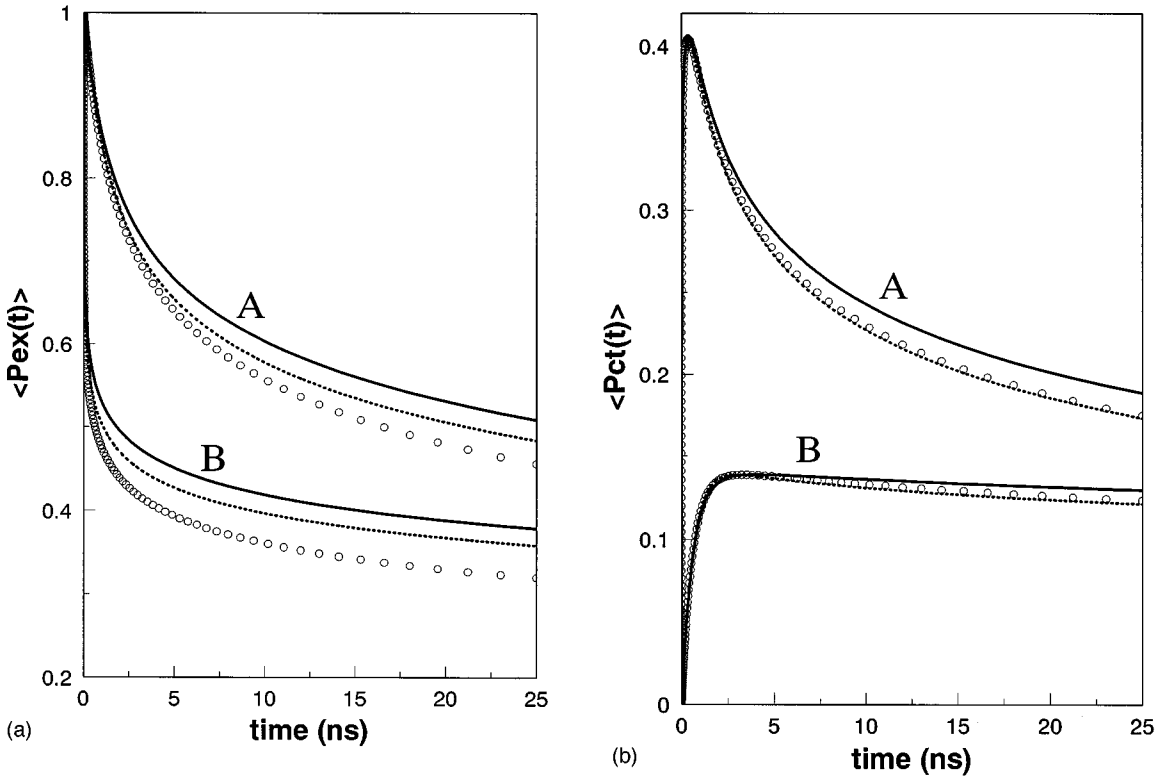

FIG. 5. $\langle P_{ex}(t)\rangle$ and $\langle P_{ct}(t)\rangle$ curves from Monte Carlo simulations (circles), the analytical point-particle theory (solid lines), and the approximate SPD theory (dashed lines) for 10% fractional occupancy. The analytical theory includes only donor–acceptor excluded volume, while the SPD method also treats acceptor–acceptor excluded volume approximately. The Monte Carlo simulations include both donor–acceptor and acceptor–acceptor excluded volume. All curves are for a 20 Å radius micelle and particle diameters of 6.8 Å (full arclength). Donor lifetime decay is not included. (a) $\langle P_{ex}(t)\rangle$ curves with parameters: Curve A: $N=13$, $R_f=10.0$ Å, $a_f=1.0$ Å, $\tau=15.0$ ns; Curve B: $N=13$, $R_f=12.0$ Å, $a_f=0.5$ Å, $\tau=15.0$ ns. (b) $\langle P_{ct}(t)\rangle$ curves with parameters: Curve A: $N=13$, $R_f=12.0$ Å, $a_f=0.5$ Å, $R_b=10.0$ Å, $a_b=1.0$ Å, $\tau=15.0$ ns; Curve B: $N=13$, $R_f=10.0$ Å$=R_b$, $a_f=1.0$ Å$=a_b$, $\tau=15.0$ ns.

find that for acceptor fractional occupancies of less than 5%, acceptor–acceptor excluded volume has a negligible effect. At fractional occupancies above 5%, the effect is on the order of that shown in Figs. 5(a) and 5(b) and can lead to observable deviations from the analytical theory, especially in the $\langle P_{ex}(t)\rangle$ curves.

For fractional occupancies greater than 5%, acceptor–acceptor excluded volume can be included in the Monte Carlo simulations. However, the lengthy run times required can make this technique prohibitive for fitting experimental data. Instead, we suggest an approximate method for including acceptor–acceptor excluded volume in the analytical theory. This approximation requires the input of the pair probability distribution for curved disks on a sphere, which may be obtained from simulation or from the approximation suggested in Appendix C. Once known, the pair probability distribution can be used to generate electron-transfer curves for any set of parameters, thereby avoiding the need to rerun the simulations whenever the parameters change. We term our approximate method the ''separable probability distribution'' (SPD) method and give details in Appendix B.

The dashed lines shown in Figs. 5(a) and 5(b) are the SPD results, calculated using the simulated pair probability distribution. As can be seen, the SPD method (dashed lines) yields good agreement with the Monte Carlo results (circles) and significantly improves the performance of the analytical theory (solid lines), especially for the $\langle P_{ct}(t)\rangle$ curves. Although the success of the SPD method in reproducing the Monte Carlo results depends on the parameters of the system, we have found that in all cases the SPD approximation is better than simply ignoring acceptor–acceptor excluded volume.

VI. CONCLUDING REMARKS

We have developed an exact theoretical treatment of photoinduced forward electron transfer and geminate recombination between one donor and N acceptors in random fixed positions on the surface of a spherical micelle. This is the first accurate treatment of forward and back electron transfer in a restricted geometry. Monte Carlo simulations of the problem with donor–acceptor excluded volume show exact agreement with the theory and demonstrate that the ensemble averages have been properly performed. The theory ceases to be rigorous only when acceptor–acceptor excluded volume is included. For fractional occupancies below 5%, this is a small effect and can be ignored. (Fractional occupancies below 5% still result in very significant amounts of electron transfer.) For higher fractional occupancies, we have suggested an approximate method for including acceptor–acceptor excluded volume in the analytical theory. A more complete discussion of this approximation is given in a separate article.[41]

Although this article treats the specific problem of molecules distributed on the surface of a sphere, the theoretical method used to treat forward and back electron transfer is general and exact for point particles with donor–acceptor excluded volume. However, the sphere problem is a special case of the general problem because the ensemble average is translationally invariant, i.e., the ensemble average about a donor located at any position on a sphere is the same. Therefore it is not necessary to perform an additional average over starting points. For systems such as polymers, this will not be the case. This has been treated extensively for the problem of electronic excitation transfer in restricted geometries.[45,46] For a system in which the ensemble average is not translationally invariant, the ensemble average is first performed over all configurations about a starting point, and then an additional average is performed over starting points. It is not sufficient to perform the average for some average starting point. The additional average over starting points will make the calculation more time consuming but does not fundamentally change the nature of the method presented above.

The results reported here are for a system in which the molecules are in fixed positions on the surface of a micelle. This may be an accurate model at sufficiently low temperatures. However, at room temperature, molecules the size of typical donors and acceptors will diffuse over significant distances on the time scale of the relevant processes.[47] This is true even when the chromophores are attached to long tails and tethered to the micelle. We are in the process of extending this work to include the effects of diffusion on photoinduced electron transfer and geminate recombination in restricted geometries.

ACKNOWLEDGMENTS

We would like to thank S. F. Swallen and Professor H. C. Andersen for extremely helpful discussions about the Monte Carlo simulations. Thanks also go to the Stanford Center for Materials Research for partial support of computing equipment. This work was supported by the Department of Energy, Office of Basic Energy Sciences (Grant No. DE-FG03-84ER13251). K.W. would like to thank the National Science Foundation for a predoctoral fellowship.

APPENDIX A: DERIVATION OF THE POINT PARTICLE PROBABILITY DISTRIBUTION, $p_{pt}(r)$

The probability that an acceptor is located distance r away from a donor at the north pole of a sphere can be derived by examining Fig. 1(B). r is the chord length, θ is the angular separation, and R is the micelle radius. r is completely determined by θ. The probability of an acceptor existing between $\theta-\Delta\theta/2$ and $\theta+\Delta\theta/2$ is simply proportional to the surface area of the circular slice traced about the z axis by r.

$$p_{pt}(\theta)d\theta=\frac{2\pi R\ \sin\ \theta}{4\pi R^2}\ R\ d\theta=\frac{\sin\ \theta}{2}\ d\theta.$$

From Fig. 1(B), $r=2R\sin(\theta/2)$ and $dr=R\cos(\theta/2)d\theta$, so that the coordinate transform gives

$$p_{pt}(r)dr=(r/2R^2)dr.$$

Note that $p(\theta)$ is peaked at $\theta=90°$, indicating that the acceptor is most likely to be found near the equator. When the probability distribution is expressed in terms of chord length, it becomes linear in r. This occurs because the surface area slice swept out between $r=r-\Delta r/2$ and $r=r+\Delta r/2$ increases with chord length for a constant Δr.

The probability distribution $p_{pt}(r)dr=r\ dr/2R^2$ is normalized over the entire surface of the sphere, i.e., from $r=0$ to $r=2R$. When donor–acceptor excluded volume is included, the acceptor can only be between r_m and $2R$, where r_m is the contact distance in chord length. Normalizing $p_{pt}(r)$ from contact to $2R$ gives

$$p_{pt}(r)dr=2r\ dr/(4R^2-R_m^2).$$

APPENDIX B: THE SPD METHOD

To include acceptor–acceptor excluded volume in the theory, we make the approximation that the N-particle probability distribution function $p(\bar{r})=p(r_1,r_2,\ldots,r_N)$ is in fact pairwise separable into N sets of identical pair probability distribution functions, $p(\bar{r})=p(r_1)p(r_2)\cdots p(r_N)=p_{aa}(r)^N$. However, $p_{aa}(r)$ is now the curved-disk pair probability function on the sphere surface, not the random distribution function for point particles on the sphere. This is related to the well-known pair distribution function, $g(r)$ by[36]

$$g(r)=p_{aa}(r)/p_{pt}(r)$$

where $p_{aa}(r)$ is the probability of having an acceptor between $r-\Delta r/2$ and $r+\Delta r/2$ when acceptor–acceptor excluded volume is included, and $p_{pt}(r)$ is the corresponding probability distribution for point particles. In general, $g(r)$ and $p_{aa}(r)$ are not known for the restricted geometry case. We note, however, that $p_{aa}(r)$ is independent of the electron-transfer parameters. Thus, once $p_{aa}(r)$ is known (e.g., by simulation) for a given micelle/donor/acceptor system of some fractional occupancy, $\langle P_{ex}(t)\rangle$ may be obtained from Eq. (7), where the hard curved disk $p_{aa}(r)$ is used in place of $p(r)$, and $\langle P_{ct}(t)\rangle$ is given by

$$\begin{aligned}\langle P_{ct}(t)\rangle=\sum_{i=1}^{N}\langle P_{ct}^{i}(t)\rangle=N\int_{r=r_m}^{2R}\int_{t'=0}^{t}k_f(r)\exp\left(\frac{-t'}{\tau}\right)\\ \times\exp[-k_f(r)t']\exp[-k_b(r)(t-t')]\\ \times\left[\int_{r'=r_m}^{2R}\exp\left[\frac{-t'}{\tau}\,e^{(R_f-r')/a_f}\right]p_{aa}(r')dr'\right]^{N-1}\\ \times dt'\ p_{aa}(r)dr.\end{aligned}\tag{B1}$$

This is the "separable probability distribution" (SPD) approximation.

The SPD equation for $\langle P_{ct}(t)\rangle$ does a very good job of reproducing the shape of the Monte Carlo simulation results, but does less well at reproducing the absolute magnitude. Any discrepancy in the magnitudes of the theoretical and simulated $\langle P_{ct}(t)\rangle$ curves, while of theoretical interest, does not affect the ability to fit experimental data, as experimental measurements of ion survival times generally have no abso-

lute magnitude associated with them.[41] Therefore, in Figs. 5(a) and 5(b), the magnitudes of both the analytical point particle theory and the SPD curves have been scaled to match the simulated curves. The SPD result significantly outperforms the analytical point particle theory and would continue to do so, even if the scaling were omitted. No similar scaling can be performed for the $\langle P_{ex}(t)\rangle$ curves.

APPENDIX C: ANALYTICAL APPROXIMATION OF $p_{aa}(r)$ FOR SAME-SIZED DONOR AND ACCEPTORS

In the SPD calculations presented in Figs. 5(a) and 5(b), we employed $p_{aa}(r)$ curves obtained from the simulations. Because obtaining $p_{aa}(r)$ in this manner requires performing a time-consuming simulation, an analytical form for $p_{aa}(r)$ is highly desirable, since the SPD method can then be employed using swift numerical methods. To this end, we suggest an extraordinarily simple approximation to $p_{aa}(r)$ for same-sized donors and acceptors on a spherical surface.

Before giving the details of the approximation, we first define the particle diameter, d, to be the end-to-end chord length across the particle, related to the full arclength, d_{arc}, by

$$d = 2R\ \sin(d_{arc}/2R),$$

where R is the micelle radius. We also define the acceptor fractional occupancy, η, as

$$\eta = \frac{N[1-\cos(d_{arc}/2R)]}{1+\cos(d_{arc}/2R)}, \tag{C1}$$

where N is the number of acceptors. (Note that the total number of particles, including the donor, is $N+1$ and that the donor arclength must equal that of the acceptor.) Equation (C1) can be readily derived by noting that the area, A, of a curved disk of full arclength d_{arc} on a sphere of radius R is $2\pi R^2[1-\cos(d_{arc}/2R)]$. The fractional occupancy for N acceptors is then defined as $N\times A/(4\pi R^2 - A)$, where we exclude the area of the donor from the area available to the acceptors.

To obtain an analytical expression for $p_{aa}(r)$, we begin by realizing that, for a fixed fractional occupancy η, $p_{aa}(r)$ can be scaled to have essentially the same functional form for all micelle and acceptor sizes. $p_{aa}(r)$ curves were obtained from Monte Carlo simulations for a variety of fractional occupancies, η. Each occupancy examined was generated in several ways by varying the micelle radius and the acceptor size and number. For a given fractional occupancy, obtained by any appropriate R, N, and d_{arc} values, the scaled $p_{aa}(r)$ curves were found to be essentially identical. Only physically reasonable R, N, and d_{arc} values and fractional occupancies up to 15% were considered.

The scaling was performed by realizing that at large distances, $p_{aa}(r)$ should approach the point-particle result, $p_{pt}(r) = 2r/(4R^2 - d^2)$ (see Appendix A). To eliminate the dependence on R and d, $p_{pt}(r)$ can be multiplied by $(4R^2-d^2)/2$, giving a scaled point particle $p_{pt}(r) = r$. We next follow the standard approach used in isotropic three dimensions[38,48] and scale $p_{pt}(r)$ by the particle diameter d, giving $p_{pt}(r/d) = (r/d)$. $p_{aa}(r)$ curves obtained from Monte Carlo simulations of the acceptor–acceptor excluded volume problem should thus have their abscissa scaled by $1/d$ and their ordinate scaled by $(4R^2-d^2)/2d$, so that they approach the point-particle result at distances beyond the correlation length. Furthermore, since the probability distributions give the probability of finding a particle between $r-\Delta r/2$ and $r+\Delta r/2$, $p_{aa}(r)$ should also be multiplied by the desired Δr.

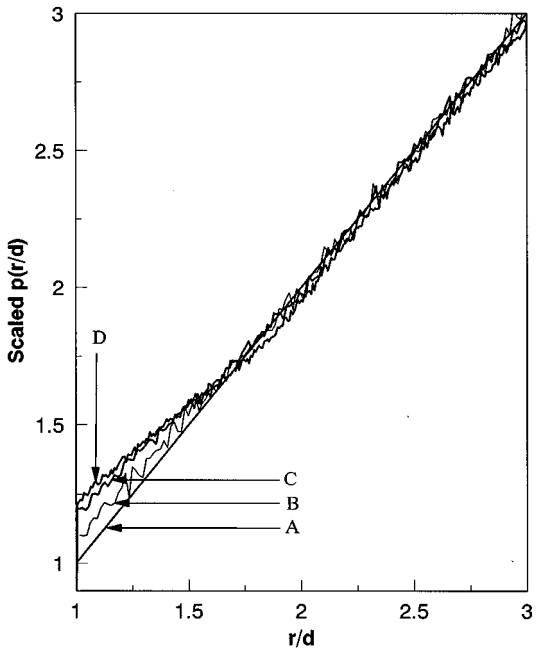

FIG. 6. $p_{aa}(r/d)$ curves obtained from Monte Carlo simulations. The curves are scaled as described in Appendix C. Curves A, B, C, and D are for fractional occupancies of 0%, 5%, 10%, and 13%, respectively. Note that the $p_{aa}(r/d)$ curves approach the point-particle result (η=0%) for large distances but deviate at short distances.

Figure 6 shows simulated $p_{aa}(r/d)$ curves scaled in this manner for various η values along with the scaled point-particle result: $p_{pt}(r/d) = (r/d)$. Note that finite-sized acceptors give scaled $p_{aa}(r/d)$ curves that depend only on η and that deviate from the point-particle line at short distances but approach a line of slope 1.0 for r/d values beyond the correlation length. Figure 6 suggests that for fractional occupancies up to 13%, $p_{aa}(r/d)$ can be closely approximated by two intersecting lines. One line reflects the short-distance interactions and has slope m_1 and intercept b_1 dependent on η. The other line is simply the point-particle result, which has slope 1.0 and intercept 0.0. Table I gives m_1 and b_1 values for fractional occupancies from 5% to 13%. For fractional occupancies below 5%, acceptor–acceptor excluded volume has a negligible effect. For fractional occupancies above 13%, $p_{aa}(r)$ develops additional structure that causes the two-line approximation to break down. Interpolating the results in Table I gives $p_{aa}(r)$ curves for intermediate η values. The approximate form of $p_{aa}(r)$ closely reproduces the simulated probability distributions, although the error begins to become significant near η=13%.

As an example, consider a system of one donor and 20 acceptors of full arclength (d_{arc}) 7.08 Å on a 25 Å radius micelle (η=10%). This corresponds to particles with a chord-length diameter of 7.056 Å. Two lines should be gen-

TABLE I. Slope (m_1) and intercept (b_1) values to use in determining approximate $p_{aa}(r)$ curves for various fractional occupancies following the method of Appendix C. The approximate $p_{aa}(r)$ curve is determined by two lines: one with slope 1.0 and intercept 0.0 and the other with slope m_1 and intercept b_1. The curves are scaled as described in Appendix C. Units for the slope are 1/Å; the intercept is dimensionless.

Fractional occupancy	m_1	b_1
5%	0.93	0.15
6%	0.88	0.23
7%	0.86	0.26
8%	0.84	0.30
9%	0.80	0.36
10%	0.79	0.39
11%	0.77	0.41
12%	0.73	0.47
13%	0.69	0.53

erated: one with slope and intercept taken from Table I and one with slope 1.0 and intercept 0.0

$$y_1 = 0.79x + 0.39, \quad y_2 = x.$$

If two files are created with (x,y) values given by these equations, then each file should have its y values multiplied by

$$\frac{2d\,\Delta r}{4R^2 - d^2} = \frac{2 \times 7.056 \times \Delta r}{4 \times 25^2 - 7.056^2} = 5.76 \times 10^{-3} \Delta r$$

and its x values multiplied by $d = 7.056$ Å. $p_{aa}(r)\Delta r$ is then given by the new scaled y_1 file for 7.056 Å$\leqslant r < r_c$ and by the scaled y_2 file for $r_c \leqslant r \leqslant 50$ Å. r_c is the value at which the two scaled lines intersect, and 50 Å is the maximum allowable distance, i.e., the acceptor is at the south pole. Δr may be any reasonable value, usually around 0.1 Å.

[1] R. A. Marcus, J. Chem. Phys. **24**, 966 (1956).
[2] R. A. Marcus, Discuss. Faraday Soc. **29**, 21 (1960).
[3] R. A. Marcus, Ann. Rev. Phys. Chem. **15**, 155 (1964).
[4] R. A. Marcus, J. Chem. Phys. **43**, 679 (1965).
[5] R. A. Marcus and N. Sutin, Biochim. Biophys. Acta. **811**, 265 (1985).
[6] T. Guarr and G. McLendon, Coordination Chem. Rev. **68**, 1 (1985).
[7] M. Inokuti and F. Hirayama, J. Chem. Phys. **43**, 1978 (1965).
[8] M. Tachiya and A. Mozumder, Chem. Phys. Lett. **28**, 87 (1974).
[9] M. Tachiya, J. Chem. Soc., Faraday Trans. II **75**, 271 (1979).
[10] M. D. Fayer, L. Song, S. F. Swallen, R. C. Dorfman, and K. Weidemaier, in *Ultrafast Dynamics of Chemical System*, edited by J. D. Simon (Kluwer Academic, Amsterdam, 1994), p. 37.
[11] Y. Lin, R. C. Dorfman, and M. D. Fayer, J. Chem. Phys. **90**, 159 (1989).
[12] M. S. Mikhelashvili, J. Feitelson, and M. Dodu, Chem. Phys. Lett. **171**, 575 (1990).
[13] N. R. Kestner, J. Logan, and J. Jortner, J. Phys. Chem. **78**, 2148 (1974).
[14] J. Jortner, J. Chem. Phys. **64**, 4860 (1976).
[15] R. P. VanDuyne and S. F. Fischer, Chem. Phys. **5**, 183 (1974).
[16] P. Siders and R. A. Marcus, J. Am. Chem. Soc. **103**, 748 (1981).
[17] A. Warshel, J. Phys. Chem. **86**, 2218 (1982).
[18] S. Chandrasekhar, Rev. Mod. Phys. **15**, 1 (1943).
[19] M. S. Mikhelashvili and M. Dodu, Phys. Lett. A **146**, 436 (1990).
[20] R. K. Huddleston and J. R. Miller, J. Phys. Chem. **86**, 200 (1982).
[21] R. P. Domingue and M. D. Fayer, J. Chem. Phys. **83**, 2242 (1985).
[22] P. Siders, R. J. Cave, and R. A. Marcus, J. Chem. Phys. **81**, 5613 (1984).
[23] S. Strauch, G. McLendon, M. McGuire, and T. Guarr, J. Phys. Chem. **87**, 3579 (1983).
[24] R. C. Dorfman, Doctoral Thesis, Stanford University, 1992.
[25] R. C. Dorfman, M. Tachiya, and M. D. Fayer, Chem. Phys. Lett. **179**, 152 (1991).
[26] *Rochester Symposium on Charge Transfer in Restricted Geometries* [J. Phys. Chem. **96**, 2777 (1991)].
[27] J. Klafter, J. M. Drake, and P. Levitz, J. Luminescence **45**, 34 (1990).
[28] M. S. Mikhelashvili and A. M. Michaeli, J. Phys. Chem. **98**, 8114 (1994).
[29] D. Devault, Q. Rev. Biophys. **13**, 387 (1980).
[30] A. H. Marcus, N. A. Diachun, and M. D. Fayer, J. Phys. Chem. **96**, 8930 (1992).
[31] K. U. Finger, A. H. Marcus, and M. D. Fayer, J. Chem. Phys. **100**, 271 (1994).
[32] J. Tobochnik and P. M. Chapin, J. Chem. Phys. **88**, 5824 (1988).
[33] G. Marsaglia and A. Zaman, J. Appl. Prob. **1**, 1 (1991).
[34] F. James, Comput. Phys. Commun. **60**, 329 (1990).
[35] M. P. Allen and D. J. Tildesley, *Computer Simulation of Liquids* (Clarendon, Oxford, 1987).
[36] J. P. Hansen and I. R. McDonald, *Theory of Simple Liquids* (Academic, London, 1976).
[37] J. P. Valleau and S. G. Whittington, in *Statistical Mechanics*, edited by B. J. Berne (Plenum, New York, 1977), Vol. 5.
[38] W. W. Wood, in *Physics of Simple Liquids*, edited by H. N. V. Temperley, J. S. Rowlinson, and G. S. Rushbrooke (Wiley, New York, 1968), p. 115.
[39] H. C. Andersen (personal communication).
[40] R. C. Dorfman, Y. Lin, M. B. Zimmt, J. Baumann, R. P. Domingue, and M. D. Fayer, J. Phys. Chem. **92**, 4258 (1988).
[41] S. F. Swallen, K. Weidemaier, and M. D. Fayer, J. Phys. Chem. (accepted for publication).
[42] H. Eyring and M. S. Jhon, *Significant Liquid Structures* (Wiley, New York, 1969).
[43] S. A. Rice and P. Gray, *The Statistical Mechanics of Simple Liquids* (Wiley, New York, 1965).
[44] D. A. McQuarrie, *Statistical Mechanics* (Harper & Row, New York, 1976).
[45] K. A. Peterson and M. D. Fayer, J. Chem. Phys. **85**, 4702 (1986).
[46] A. H. Marcus, M. D. Fayer, and J. G. Curro, J. Chem. Phys. **100**, 9156 (1994).
[47] E. L. Quitevis, A. H. Marcus, and M. D. Fayer, J. Phys. Chem. **97**, 5762 (1993).
[48] G. J. Throop and R. J. Bearman, J. Chem. Phys. **42**, 2408 (1964).